



## Comparison of the Empirical Ionospheric Models During Three Severe Geomagnetic Storm Occurred in 2015

Selçuk SAĞIR<sup>1</sup>, Şerife ERBAY<sup>1</sup>

<sup>1,2</sup> Department of Physics, Art and Science Faculty, Mus Alparslan University, Muş, Türkiye

✉: [s.sagir@alparslan.edu.tr](mailto:s.sagir@alparslan.edu.tr)  0000-0002-5698-0154  0000-0002-9749-5403

Received (Geliş): 16. 09.2022

Revision (Düzelme):10.11.2022

Accepted (Kabul): 07.12.2022

### ABSTRACT

The geomagnetic field acts as both the shield and the electron density regulator for the ionosphere. The effect of the geomagnetic field on the ionosphere can be examined separately for the geomagnetically quiet and disturbed days. In the current study, the performance of the ionospheric models was evaluated for three different severe geomagnetic storms periods during the year of 2015, which was in the beginning of the descending phase of the 24<sup>th</sup> solar cycle. These three storms occurred during 17-18 March, 22-23 June and 20-21 December of year 2015 in which first one expressed as St. Patrick's Day geomagnetic storm. The relationship between Total Electron Content (TEC) was measured by Global Positioning System (GPS) and evaluated with NeQuick 2, IRI 2016, IRI Plas (without any input- "IRI Plas") and IRI Plas TEC (with TEC input- "IRI Plas TEC") global models at three Turkey IGS station namely Ankara (39.57 N, 32.53 E), Istanbul (40.58 N, 29.05 E) and Erzurum (40.39 N, 40.42 E) investigated. The comparison was made separately for pre-storm, during storm and post-storm by using the Mean Absolute Error (MAE), Root Mean Square Error (RMSE) and Mean Absolute Percentage Error (MAPE) metrics and symmetric Kullback-Leibler Distance (KLD) methods. Among the empirical models, IRI Plas TEC is generally present to be better results than other models for all storm processes. It can be stated that IRI 2016 is better in the storm return phase compared to other phases of the storm.

**Keywords:** IRI 2016, IRI Plas, NeQuick 2 Model, Total Electron Content

### 2015 Yılında Meydana Gelen Üç Şiddetli Jeomanyetik Fırtına Süresince Deneysel İyonosferik Modellerin Karşılaştırılması

#### ÖZ

Jeomanyetik alan, iyonosfer için hem kalkan hem de elektron yoğunluk düzenleyicisi görevi görür. Jeomanyetik alanın iyonosfer üzerindeki etkisi, sakin ve fırtınalı günler için ayrı ayrı incelenebilir. Bu çalışmada, 24. güneş devrinin azalan fazının başlangıcı olan 2015 yılı boyunca iyonosferik modellerin performansı üç farklı şiddetli jeomanyetik fırtına dönemi için değerlendirilmiştir. Bu üç fırtına, 2015 yılının 17-18 Mart, 22-23 Haziran ve 20-21 Aralık tarihlerinde meydana gelmiş ve bunlardan ilki St. Patrick Günü jeomanyetik fırtınası olarak ifade edilir. Toplam Elektron İçeriği (TEC) arasındaki ilişki Küresel Konumlandırma Sistemi (GPS) ile ölçülmüş ve NeQuick 2, IRI 2016, IRI Plas (herhangi bir giriş olmadan- "IRI Plas") ve IRI Plas TEC (TEC girişi ile- "IRI Plas TEC") ile değerlendirilmiştir. Ankara (39.57 K, 32.53 D), İstanbul (40.58 K, 29.05 D) ve Erzurum (40.39 K, 40.42 D) olmak üzere üç Türkiye IGS istasyonunda küresel modeller incelenmiştir. Karşılaştırma, Ortalama Mutlak Hata (MAE), Ortalama Kare Hata (RMSE) ve Ortalama Mutlak Yüzde Hata (MAPE) metrikleri ve simetrik Kullback-Leibler Mesafesi (KLD) kullanılarak fırtına öncesi, fırtına sırasında ve fırtına sonrası için ayrı ayrı yapılmıştır. Ampirik modeller arasında IRI Plas TEC, tüm fırtına süreçleri için genel olarak diğer modellerden daha iyi bulunmuştur. IRI 2016'nın fırtına dönüş aşamasında fırtınanın diğer aşamalarına göre daha iyi olduğu ifade edilebilir.

**Anahtar Kelimeler:** IRI 2016, IRI Plas, NeQuick 2 Model, Toplam Elektron içeriği

#### INTRODUCTION

The ionosphere is the region that starts at an altitude of about 50 km from the earth and extends to an altitude of 1000 km. This region is measured with tools such as scattering radar, ionosonde and satellite-GPS

communication. These devices, especially the ionosonde and scattering radar, are not available to a very common installation network due to the high cost of installation and maintenance. Ionospheric medium outside the installation areas are modeled with empirical models such as IRI and NeQuick 2 and many models such as

ARIMA, machine learning, deep learning, experimental orthogonal analysis [1–6].

The ionospheric medium is studied by the total electron content (TEC), which refers to the electron content in the beam path between the satellite and the receiver. These TEC values can be obtained by GPS-based measurement methods as well as empirical models. IRI, which is the most comprehensive and widely used model among these empirical models, provides the parameter many ionospheric ion concentrations (O+, H+, He+, N+, NO+, O+2, Cluster ions), equatorial vertical ion drift, vertical ionospheric electron content (VTEC)[6–9].

The IRI model calculates TEC up to a maximum of 10000 km, ion temperature, electron temperature, etc up to 2000 km. To calculate TEC and electron density (Ne), these heights were extended by the IRI-PLAS model up to the upper limit of 20200 km[10–12]

Another empirical ionospheric model, the NeQuick model, is based on the DGR model developed by Di Giovanni and Radicella (1990) [2]. The NeQuick is an experimental model chosen as the ionospheric delay correction model of GALILEO single frequency receivers [13, 14]. The model has a simpler and simpler use than models such as Global Assimilation of Ionospheric Measurements (GAIM) and Electron Density Assimilative Model (EDAM) [15]. The NeQuick model provides the electron density values for the altitude value determined by entering the desired latitude and longitude value. It also provides the TEC values in a beam path between the satellite and the GPS for the given latitude and longitude value. For all these values, it also includes the number of sunspots and the F10.7 solar flux values [16–18].

There are many models that evaluate the performance of any given model. In this study, the relation between the TEC values measured by GPS and TEC obtained from the NeQuick 2, IRI-2016 and IRI-PLAS model at Ankara (39.57 N, 32.53 E), Istanbul (40.58 N, 29.05 E) and Erzurum (40.39 N, 40.42 E) stations for three different magnetic storm processes that occurred during the year of 2015 investigated. The reason for choosing these stations is that they are located on almost the same latitude and allow to evaluate the results of a longitudinal change. TEC values obtained were compared using the Mean Absolute Error (MAE), Root Mean Square Error (RMSE), Mean Absolute Percentage Error (MAPE) methods and Symmetric Kullback-Leibler Distance (KLD) methods, which are widely used in ionospheric model comparisons [19–21].

## MATERIALS AND METHODS

The performance of the empirical models during the storm process, 72 hours before and 72 hours after the main phase of three different severe geomagnetic storms that occurred in March, June and December in 2015, the beginning of the descending phase of the 24<sup>th</sup> solar cycle were evaluated. 1<sup>st</sup> storm 17-18 March 2015 Patrick's Day geomagnetic storm[31], 2<sup>nd</sup> storm 22-23 June 2015 geomagnetic storm[32] and 3<sup>rd</sup> storm 20-21 December geomagnetic storm [33] occurred.

Measured TEC data is taken as Rinex file from TNPNGN-Active, Turkish National Permanent GPS Network. Then, these data were turned into regular data through the system established within the Department of Electrical and Electronics of Hacettepe University and called “<http://www.ionolab.org/>” on the internet[22–24]. IRI 2016 TEC data is taken by choosing Ne F-peak(CCIR), F-peak storm model (on) to optional input values. No other changes were made in the opened interface window[6, 25]. IRI Plas TEC values were obtained in two different ways, without making any changes to the opened interface and by simply selecting TEC in the Solar Proxy Index in the opened interface[12, 26, 27]. Geomagnetic indices are taken from <https://omniweb.gsfc.nasa.gov>, which is operating within NASA. NeQuick 2 model data is taken from the web interface of the model, <https://t-ict4d.ictp.it/NeQuick2>[18]. All TEC data were obtained in universal time (UT) for altitudes between 110 km and 10000 km and comparisons were made as hourly values. The statistical metrics and Symmetric Kullback-Leibler Distance (KLD) given below were used to compare the GPS TEC values with the empirical models TEC (NeQuick 2 TEC, IRI 2016 TEC, IRI-Plas without any input (IRI Plas), IRI-Plas with TEC input (IRI Plas (TEC))) values.

### Mean Absolute Error

$$MAE = \frac{1}{n} \sum_j^n |e_j| \quad (1)$$

### Root Mean Square Error

$$RMSE = \sqrt{\frac{\sum_j^n e_j^2}{n}} \quad (2)$$

### Mean Absolute Percent Error

$$MAPE = \frac{100}{n} \sum_j^n \frac{|e_j|}{|A_j|} \quad (3)$$

In this equations, n represents the number of samples, e<sub>j</sub> is the difference of the measurement value from the model value, and A<sub>j</sub> is the measurement value [19, 28].

### Symmetric Kullback-Leibler Distance (KLD)

In statistical comparisons, the symmetric Kullback-Leibler Distance (KLD) is widely used to identify similarities and differences between two possible density distributions [21, 29, 30]. In order to compare the measured TEC values obtained hourly from different empirical models is normalized to its value at time t for u the empirical model or the measured TEC value by equation 4.

$$\hat{P}_{u;t} = \mathbf{x}_{u;d} \left[ \sum_{n=N_i}^{N_s} \mathbf{x}_{u;d}(n) \right]^{-1} \quad (4)$$

where d represents the hourly TEC values. N<sub>s</sub> ve N<sub>i</sub> indicate the start and end values of the investigated storm phase (pre, during and post), respectively.

$$KL(\hat{P}_{u;d} \setminus \hat{P}_{v;d}) = \sum_{n=N_i}^{N_s} \hat{P}_{u;d}(n) \ln \left( \frac{\hat{P}_{u;d}(n)}{\hat{P}_{v;d}(n)} \right) \quad (5)$$

$$KL(\hat{\mathbf{P}}_{v;d} \setminus \hat{\mathbf{P}}_{u;d}) = \sum_{n=N_i}^{N_s} \hat{P}_{v;d}(n) \ln \left( \frac{\hat{P}_{v;d}(n)}{\hat{P}_{u;d}(n)} \right) \quad (6)$$

where  $N_i < n < N_s$ . "u" stands for NeQuick model TEC values, and "v" stands for TEC values for the other empirical model used in the comparison. The symmetric Kullback-Leibler distance is defined as the sum of the Kullback-Leibler divergences [21, 29].

$$KLD(\hat{\mathbf{P}}_{v;d}; \hat{\mathbf{P}}_{u;d}) = KL(\hat{\mathbf{P}}_{u;d} \setminus \hat{\mathbf{P}}_{v;d}) + KL(\hat{\mathbf{P}}_{v;d} \setminus \hat{\mathbf{P}}_{u;d}) \quad (7)$$

## RESULTS AND DISCUSSION

The performance of the models was evaluated for three different severe geomagnetic storm periods in 2015.

### Determination of Geomagnetic Storm Processes

The variation of geomagnetic indices over time of the investigated geomagnetic storm processes is shown in Figures 1, 2, and 3.

Figure 1 shows the temporal variation of geomagnetic indices for the 17-18 March 2015 storm process known in the literature as St. Patrick's Day geomagnetic storm[34]. A geomagnetic storm began at approximately 04:45 UT on March 17, when a coronal mass discharge (CME) hit Earth's magnetic field. Initially, the Interplanetary Magnetic Field (IMF) Bz component went north for a time, reaching ~27 nT, and the storm made a sudden storm commencement before turning south by about 06:00 UT. The storm reached peak (severe) intensity at ~00:00 UT on March 18 with a minimum Dst of ~-223 nT and recovered on March 25. Initial phase starting at 07:00 UT on 16 March (IMF-Bz = 10 nT,  $kp^*10=37$ , Dst = 2 nT) continued until 17 March 06:00 UT (IMF-Bz = 19 nT,  $kp^*10=47$ , Dst = 56 nT). The storm main phase that started from this moment continued until 17 March 22:00 UT (IMF-Bz = -15.5 nT,  $kp^*10=77$ , Dst = -223 nT). Then the storm return phase started. This phase lasted until 20 March 12:00 UT (IMF-Bz = 0.1 nT,  $kp^*10=27$ , Dst = -48 nT) [34, 35].

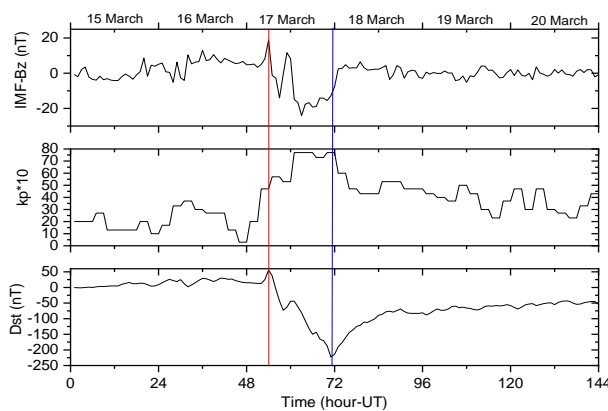


**Figure 1.** Temporal variation of geomagnetic indices for 1<sup>st</sup> storm days.

The storm began in June 2015 with two CMEs hitting the Earth at ~5:45 UT and ~18:38 UT on 22 June 2015. The solar speed increased from ~450 to ~700 km/s and pressure from 7 to 55 nPa. The IMF Bz fluctuated from

southward/northward from ~19:20 UT on 22 June to ~08 UT on 23 June. It remained southward for longest duration from 08 UT to 12 UT on 23 June 2015, which caused minimum Dst of ~ -204 nT at ~4:30 UT on 23 June 2015[36].

Figure 2 shows the time change of geomagnetic indices for the 2<sup>nd</sup> storm period. Initial phase starting 21 June at 15:00 UT (IMF-Bz = -0.1 nT,  $kp^*10=10$ , Dst = 2 nT), continued until 22 June 06:00 UT (IMF-Bz = -3.1 nT,  $kp^*10=43$ , Dst = 13 nT). The storm main phase that started from this moment continued until 23 June 04:00 UT (IMF-Bz = -20.8 nT,  $kp^*10=77$ , Dst = -204 nT). Then the storm return phase started. This phase lasted until 24 June 19:00 UT (IMF-Bz = 1.7 nT,  $kp^*10=27$ , Dst = -47 nT) [37].

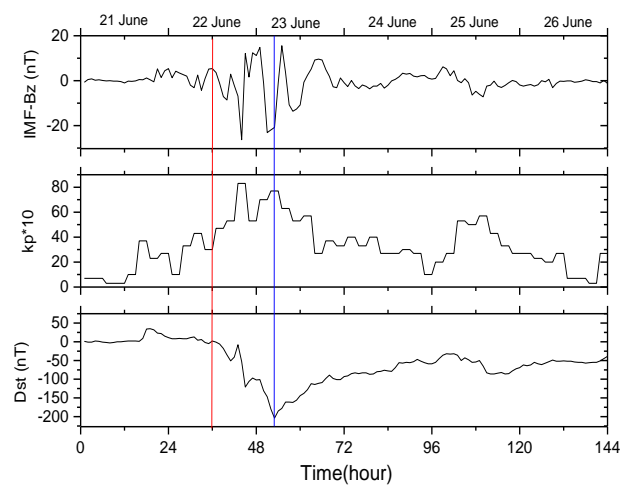


**Figure 2.** Temporal variation of geomagnetic indices for 2<sup>nd</sup> storm days.

A strong geomagnetic storm (level G3) occurred on 19–21 December 2015. This storm was initiated as a result of a class C6 solar flare and two coronal mass ejections that occurred on December 16, 2015. It reached Earth's magnetosphere on December 19, 2015, when a sudden increase in the parameters of the solar wind and interplanetary magnetic field (IMF) was recorded. The sudden onset of storm (SSC) was recorded on December 19, 2015 at ~16:16 UT. Shortly after the shock, the IMF vertical component (Bz) moved strongly southward to -10 nT, a few minutes later the IMF Bz turned north and reached ~14 nT at 17:07 UT[38].

Figure 3 shows the time change of geomagnetic indices for the 3<sup>rd</sup> storm period. Initial phase starting at 11:00 UT on December 19 (IMF-Bz = -0.1 nT,  $kp^*10=10$ , Dst = 5 nT) continued until December 19 at 23:00 UT (IMF-Bz = 2.2 nT,  $kp^*10=40$ , Dst = 40 nT). The storm main phase, which started from this moment, continued until December 20, 22:00 UT (IMF-Bz = -17.8 nT,  $kp^*10=6.3$ , Dst = -155 nT). Then the storm return phase started. This phase lasted until 21 December 21:00 UT (IMF-Bz = 0.9 nT,  $kp^*10=13$ , Dst = -38 nT) [33, 38, 39].

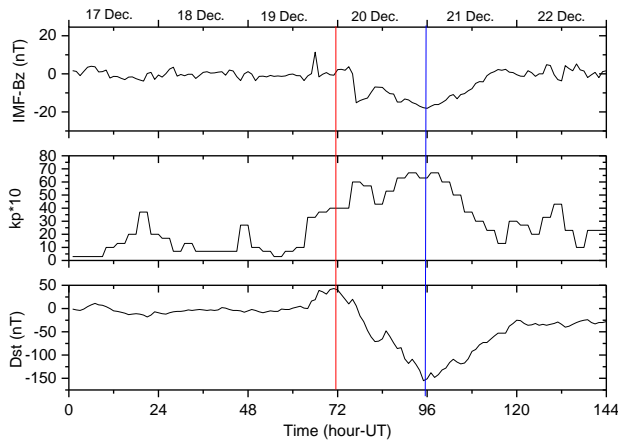


**Figure 3.** Temporal variation of geomagnetic indices for 3<sup>rd</sup> storm days.

### Analysis results for Ankara station

The temporal variation of the measured TEC and TEC obtained from NeQuick 2 model, IRI 2016, IRI Plas, IRI

Plas TEC models at Ankara station for the 1<sup>st</sup> Storm is shown in Figure 4. The evaluation results of the model (by using Equations (1), (2), (3) and (7)) are given in Table 1. The variation of NeQuick 2 values generally shows a similar distribution for the whole examined time. It is observed that the difference between the distribution of NeQuick 2 TEC and the measured value increases in the main phase of the storm and decreases in the return phase. The highest similar distribution of NeQuick 2 and IRI 2016 model TEC values can be understood from the metric models and the KLD model. The reason for this may be that both models make ionospheric topside estimations with the same method. During the storm, the weakest correlation was observed between NeQuick 2 and measured TEC values in both MAE and RMSE metrics and KLD value, except for MAPE value. The best agreement with the measured TEC value for all storm conditions is between IRI Plas and IRI Plas TEC.

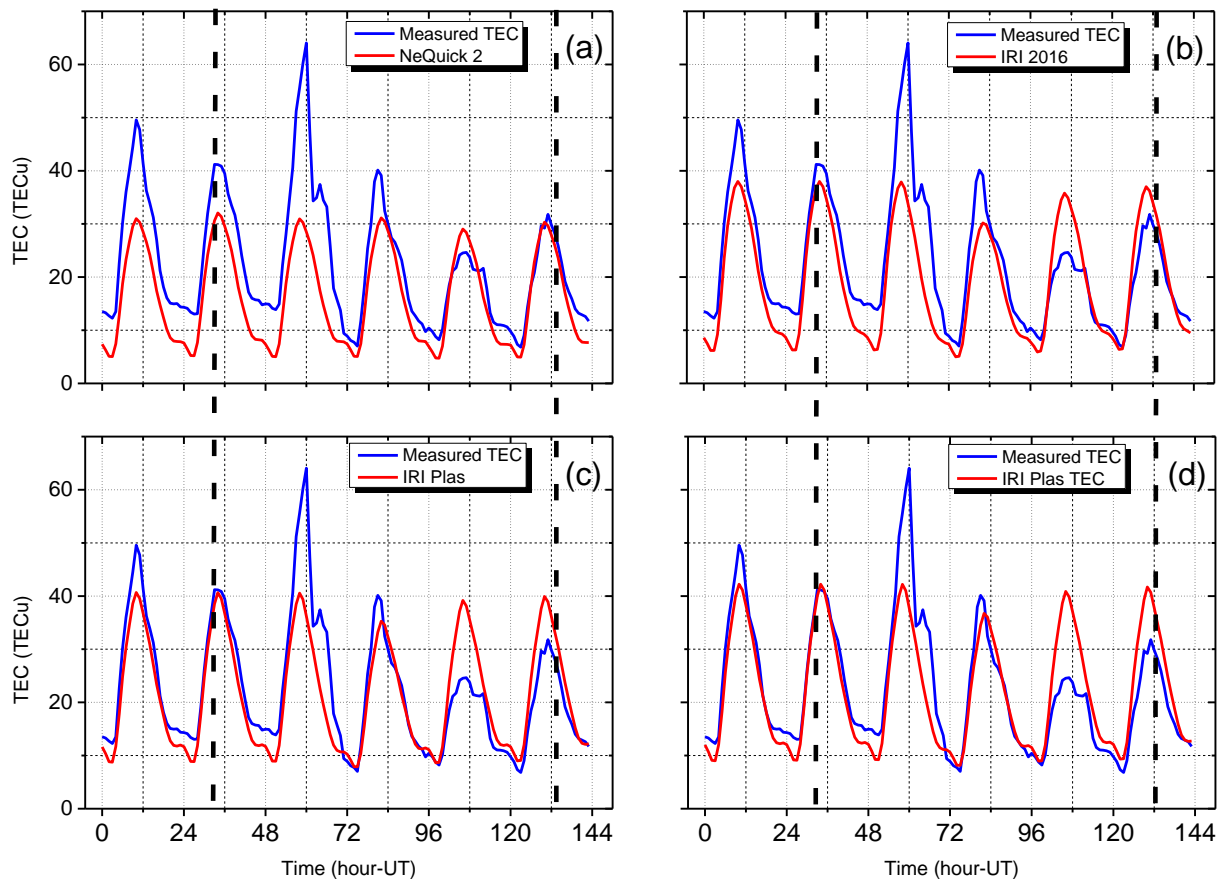


**Figure 4.** Variation of measured- NeQuick 2 TEC (a), Measured - IRI 2016 TEC (b), Measured - IRI Plas TEC (c), Measured - IRI Plas TEC (d) for 1<sup>st</sup> geomagnetic storm at Ankara station. The duration between the dashed black lines indicates the storm time

**Table 1.** Comparison results for the 1<sup>st</sup> geomagnetic storm process at Ankara station

	Measured -NeQuick 2			Measured - IRI-2016			Measured - IRI-Plas			Measured - IRI-Plas (TEC)		
	pre-storm	during storm	post storm	pre-storm	during storm	post storm	pre-storm	during storm	post storm	pre-storm	during storm	post storm
MAE	9,28	7,55	1,28	5,92	6,68	0,68	3,65	5,69	0,14	2,88	5,64	0,10
RMSE	9,78	11,82	2,46	6,15	10,81	1,31	4,11	9,96	0,27	3,35	9,86	0,31
MAPE	42,55	29,97	24,10	29,45	25,99	13,58	16,78	21,43	13,96	13,67	22,22	17,92
KLD	0.022	0.101	0.020	0.024	0.112	0.015	0.006	0.108	0.019	0.007	0.108	0.018

The temporal variation of TEC values measured and obtained with empirical models is shown in Figure 5 for the 2<sup>nd</sup> geomagnetic storm process. The evaluation results of the model (by means of Equations (1), (2), (3) and (7)) are given in Table 2. The distribution curves are quite similar while there are the amplitude differences of these changes. In the KLD analysis model, it is seen that KLD takes small values in all comparisons. However, the largest values in the KLD and RMSE and MAE metrics were calculated throughout the storm, except for the

weak relations NeQuick 2 –measured. When the MAPE metric results and the pairwise comparisons are examined, it is seen that there are values that can be expressed well. In this respect, the results are consistent with [16]. The RMSE value is a measure of the errors of the predictive model. If the MAPE value is < 10, it is considered an excellent model, and if the value is < 20, it is considered a good model result indicator [19].

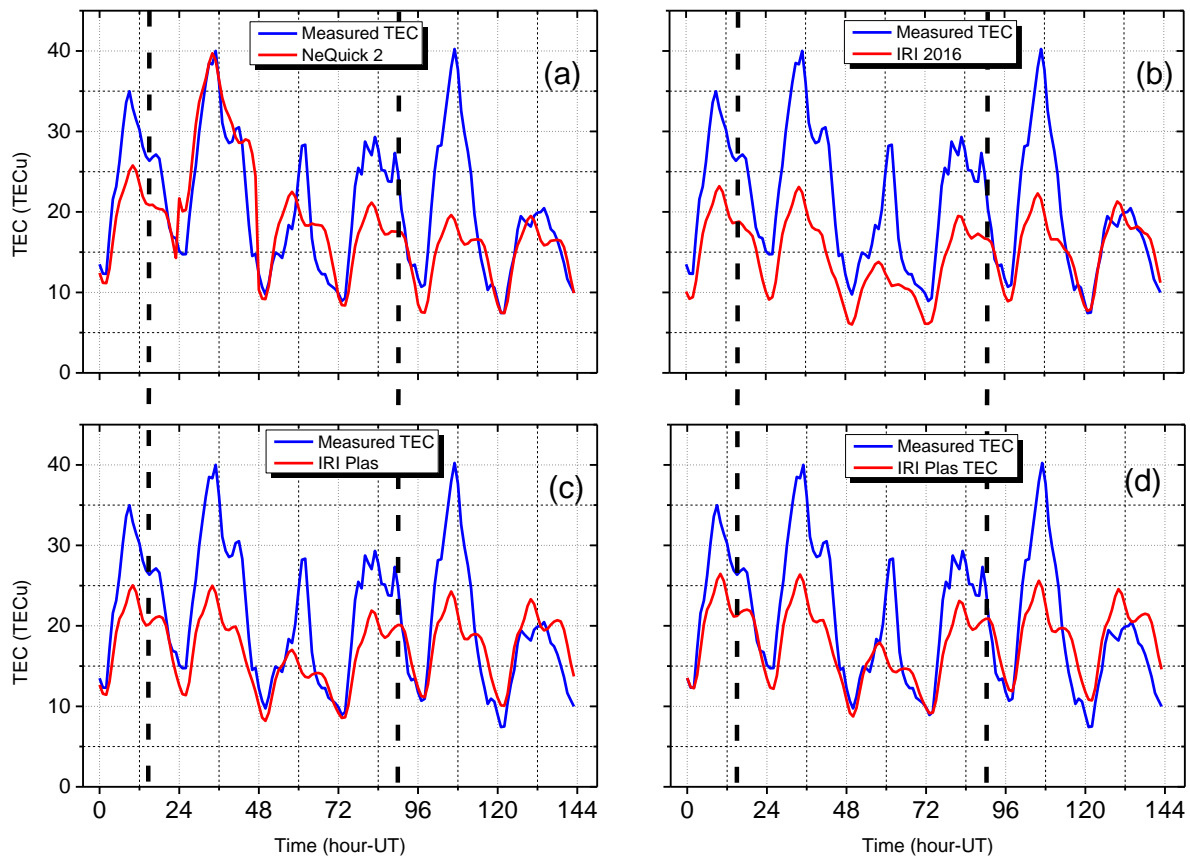


**Figure 5.** Variation of measured- NeQuick 2 TEC (a), Measured - IRI 2016 TEC (b), Measured - IRI Plas TEC (c), Measured - IRI Plas TEC (d) for Ankara station during 2<sup>st</sup> geomagnetic storm. The duration between the dashed black lines indicates the storm time

**Table 2.** Comparison results for the 2<sup>nd</sup> geomagnetic storm process at Ankara station

	Measured -NeQuick 2			Measured - IRI-2016			Measured - IRI-Plas			Measured - IRI-Plas (TEC)		
	pre-storm	during storm	post storm	pre-storm	during storm	post storm	pre-storm	during storm	post storm	pre-storm	during storm	post storm
MAE	5,81	4,45	4,86	8,27	7,95	4,22	6,33	5,58	4,48	5,14	4,90	4,78
RMSE	6,28	5,35	7,51	8,57	8,99	6,55	6,94	7,02	6,09	5,84	6,29	5,94
MAPE	21,56	22,30	20,67	32,26	34,98	17,99	22,98	22,33	22,70	18,03	19,45	26,08
KLD	0.002	0.031	0.042	0.003	0.023	0.068	0.008	0.030	0.083	0.008	0.030	0.082

Figure 6 shows the temporal change of TEC values measured and obtained from the empirical models TEC for the 3<sup>rd</sup> geomagnetic storm process. The evaluation results of the model (by using Equations (1), (2), (3) and (7)) are given in Table 3. While the TEC values measured during the storm show an increase and fluctuations at noon, it is seen that the increases occur while the fluctuations are not observed in the empirical models.

When the KLD analysis and metrics were examined It is seen that empirical models give more successful results in the pre-storm period, but this success rate decreases during and post storm. When the metric values are examined, it is seen that there is a better relationship between the IRI Plas TEC values and the measurement values.

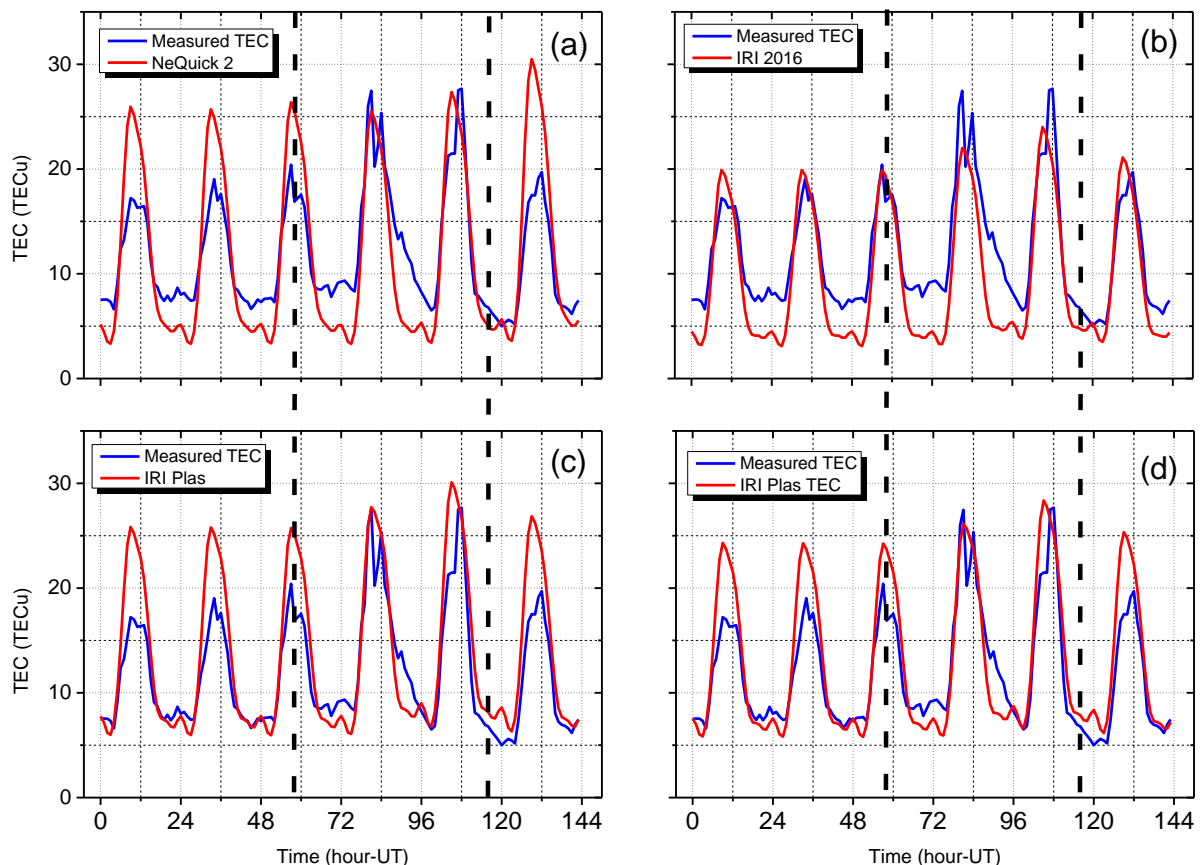


**Figure 6.** Variation of measured- NeQuick 2 TEC (a), Measured - IRI 2016 TEC (b), Measured - IRI Plas TEC (c), Measured - IRI Plas TEC (d) for 3<sup>rd</sup> geomagnetic storm at Ankara station. The duration between the dashed black lines indicates the storm time

**Table 3.** Comparison results for the 3<sup>rd</sup> geomagnetic storm process at Ankara station

	Measured -NeQuick 2			Measured - IRI-2016			Measured - IRI-Plas			Measured - IRI-Plas (TEC)		
	pre-storm	during storm	post storm	pre-storm	during storm	post storm	pre-storm	during storm	post storm	pre-storm	during storm	post storm
MAE	3,72	3,51	3,79	2,77	3,69	1,88	2,81	2,59	3,20	2,34	2,37	2,58
RMSE	4,36	3,98	5,41	2,99	4,24	2,09	4,03	3,33	4,14	3,26	2,87	3,39
MAPE	33,74	30,10	30,58	31,20	31,66	22,02	20,41	19,76	30,66	17,76	18,24	25,30
KLD	0.005	0.063	0.086	0.003	0.023	0.068	0.008	0.030	0.083	0.008	0.031	0.0082

**Analysis results for Erzurum station**

The variation of the measured and empirical model TEC values obtained for Erzurum station for the 1<sup>st</sup> storm was shown in Figure 7. The evaluation results of the model (by means of Equations (1), (2), (3) and (7)) are given in Table 4. When the measured values are examined, an increase in TEC values is observed, especially with the main phase of the storm. Then, it was started to decrease with the return phase. While this increase was not observed in the empirical models examined, the decrease

was observed in other models except NeQuick 2. Especially small KLD values indicate the existence of a positive correlation between the measured and empirical models, while higher results in the obtained values during main phase indicate the aspects that need improvement of the empirical models. The fact that the MAPE Metric values obtained by using the IRI Plas and IRI Plas TEC models for the periods outside the main phase of the storm are less than 20 indicates that the performance of the models is good.

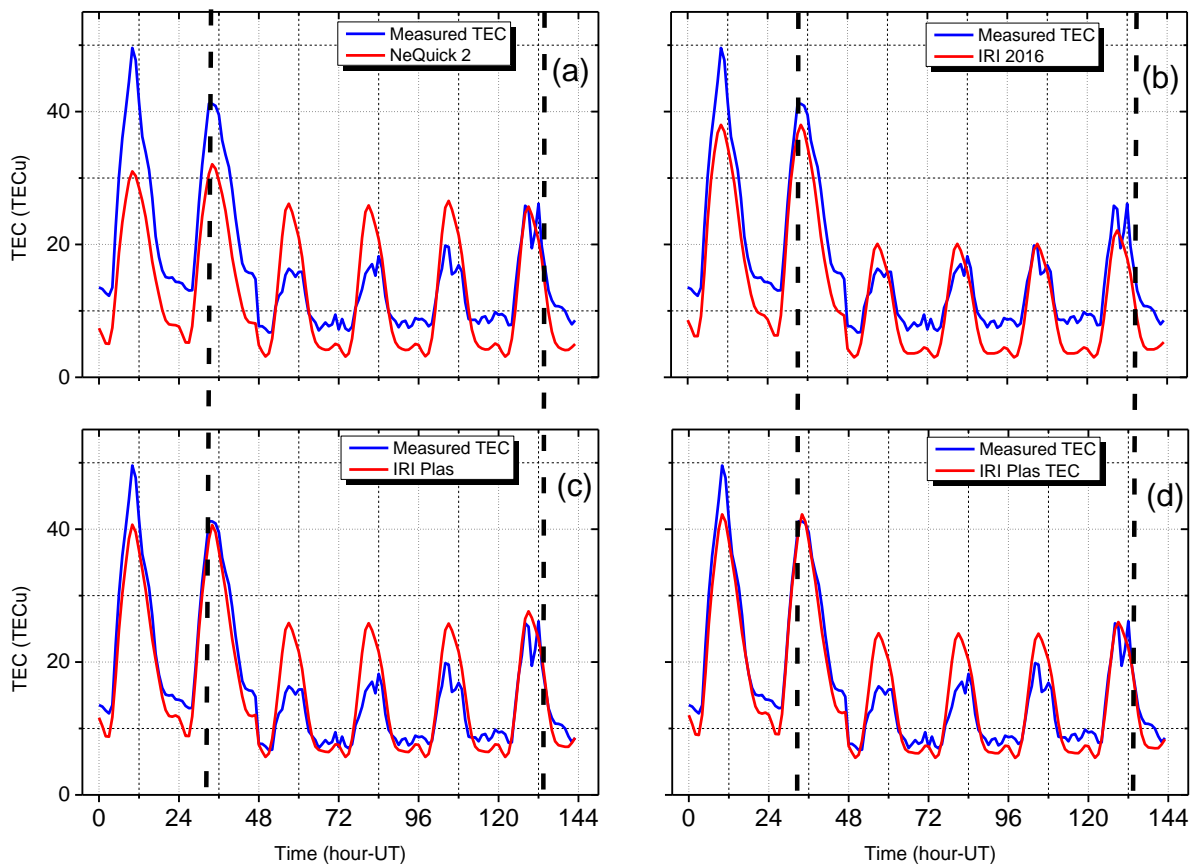


**Figure 7.** Variation of measured- NeQuick 2 TEC (a), Measured - IRI 2016 TEC (b), Measured - IRI Plas TEC (c), Measured - IRI Plas TEC (d) for the 1<sup>st</sup> geomagnetic storm at Erzurum station. The time duration between the dashed black lines indicates the storm time

**Table 4.** Comparison results for the 1<sup>st</sup> geomagnetic storm process at Erzurum station

	Measured -NeQuick 2			Measured - IRI-2016			Measured - IRI-Plas			Measured - IRI-Plas (TEC)		
	pre-storm	during storm	post storm	pre-storm	during storm	post storm	pre-storm	during storm	post storm	pre-storm	during storm	post storm
MAE	9,28	6,72	1,50	5,94	6,02	1,02	3,81	4,86	0,35	3,13	4,77	0,22
RMSE	9,56	8,69	2,88	6,17	7,78	1,95	4,14	7,13	0,68	3,47	7,19	0,44
MAPE	43,53	31,96	26,68	30,66	29,43	18,90	18,88	22,50	17,09	16,15	22,63	19,60
KLD	0,036	0,092	0,035	0,040	0,103	0,056	0,012	0,082	0,017	0,012	0,086	0,034

Figure 8 shows the temporal variation of both measured and empirical models TEC values for the 2<sup>nd</sup> storm process. The evaluation results of the model (by Equations (1), (2), (3) and (7)) are given in Table 5. When the curves are examined, it is observed that NeQuick 2 TEC values consisted of the measured values, especially pre and post storm time. When the statistical metric results given in Table 5 are examined, it is seen that during the storm, both metrics (RMSE and MAPE)

and KLD values are higher than the pre and post storm times. In addition, the fact that MAPE values are less than 20 in these processes shows that the NeQuick 2 model is a good model for this storm process [16, 21]. It is possible to express the IRI Plas TEC model as a good model, since the metrics and KLD values are quite small and the MAPE values are less than 20.

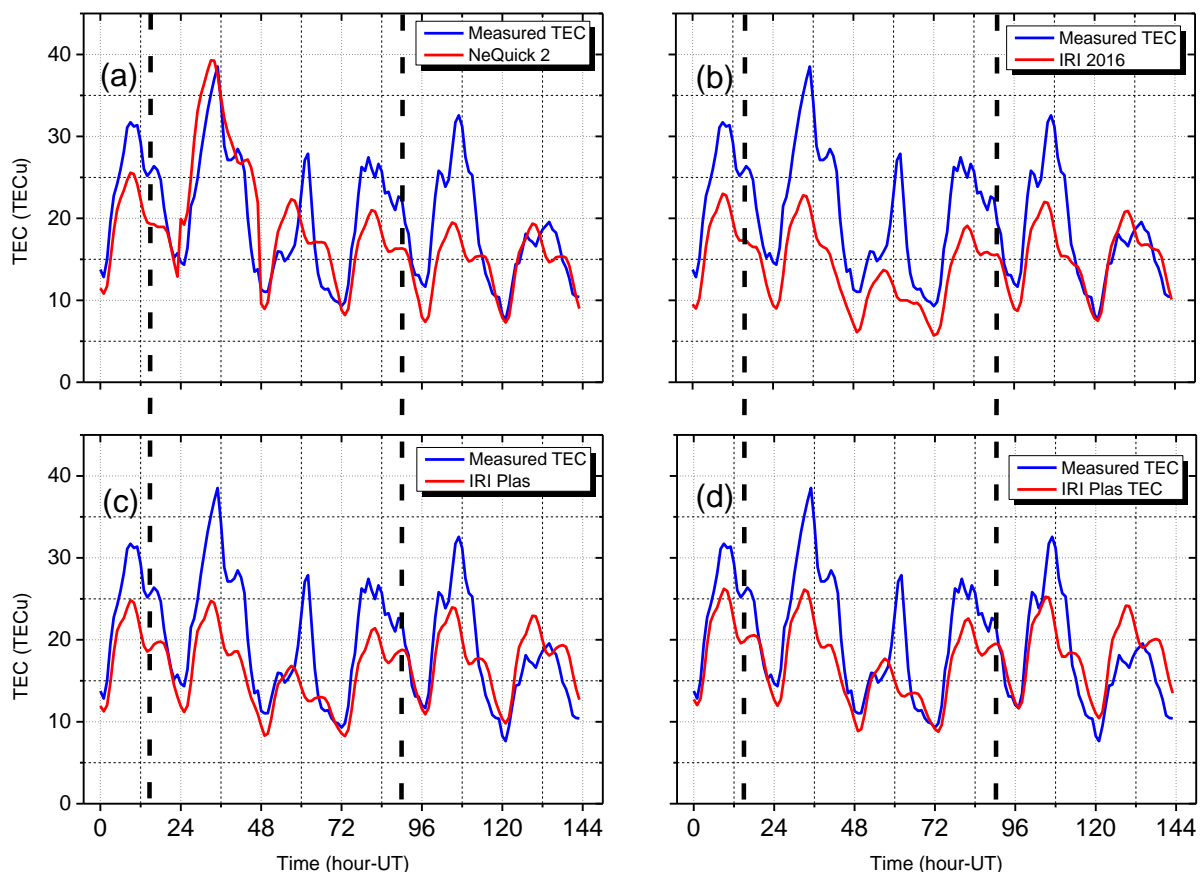


**Figure 8.** Variation of measured- NeQuick 2 TEC (a), Measured - IRI 2016 TEC (b), Measured - IRI Plas TEC (c), Measured - IRI Plas TEC (d) for the 2<sup>nd</sup> geomagnetic storm at Erzurum station. The time duration between the dashed black lines indicates the storm time



**Table 5.** Comparison results for the 2<sup>nd</sup> geomagnetic storm process at Erzurum station

	Measured -NeQuick 2			Measured - IRI-2016			Measured - IRI-Plas			Measured - IRI-Plas (TEC)		
	pre-storm	during storm	post storm	pre-storm	during storm	post storm	pre-storm	during storm	post storm	pre-storm	during storm	post storm
MAE	5,11	4,50	4,01	7,53	7,33	3,43	5,61	5,04	3,48	4,42	4,40	3,63
RMSE	5,21	5,21	5,62	7,53	8,25	4,71	5,86	6,33	4,37	4,74	5,65	4,40
MAPE	20,63	23,33	19,63	30,91	34,15	17,11	22,07	21,59	19,80	17,09	18,79	22,02
KLD	0.002	0.064	0.058	0.001	0.026	0.045	0.003	0.031	0.054	0.004	0.031	0.053

Figure 9 shows the temporal variation of TEC values obtained by measured and obtained with empirical models for the 3<sup>rd</sup> storm at Erzurum station. The evaluation results of the model (by using Equations (1), (2), (3) and (7)) are given in Table 6. It has been observed that the NeQuick 2 model TEC values provide exaggerated values before and after the storm, and this exaggeration is approximately equivalent to the increase in the TEC caused by the storm. However, the high values of the MAPE metric and KLD also indicate a weak

relationship between the NeQuick 2 model TEC and the measured TEC. Unlike other storm processes for this station, model performance appears to be better during the main phase of the storm during this storm period. Considering that the TEC values increase during the main phase of the storm, it is observed that the model values actually make a higher prediction for the non-storm conditions.

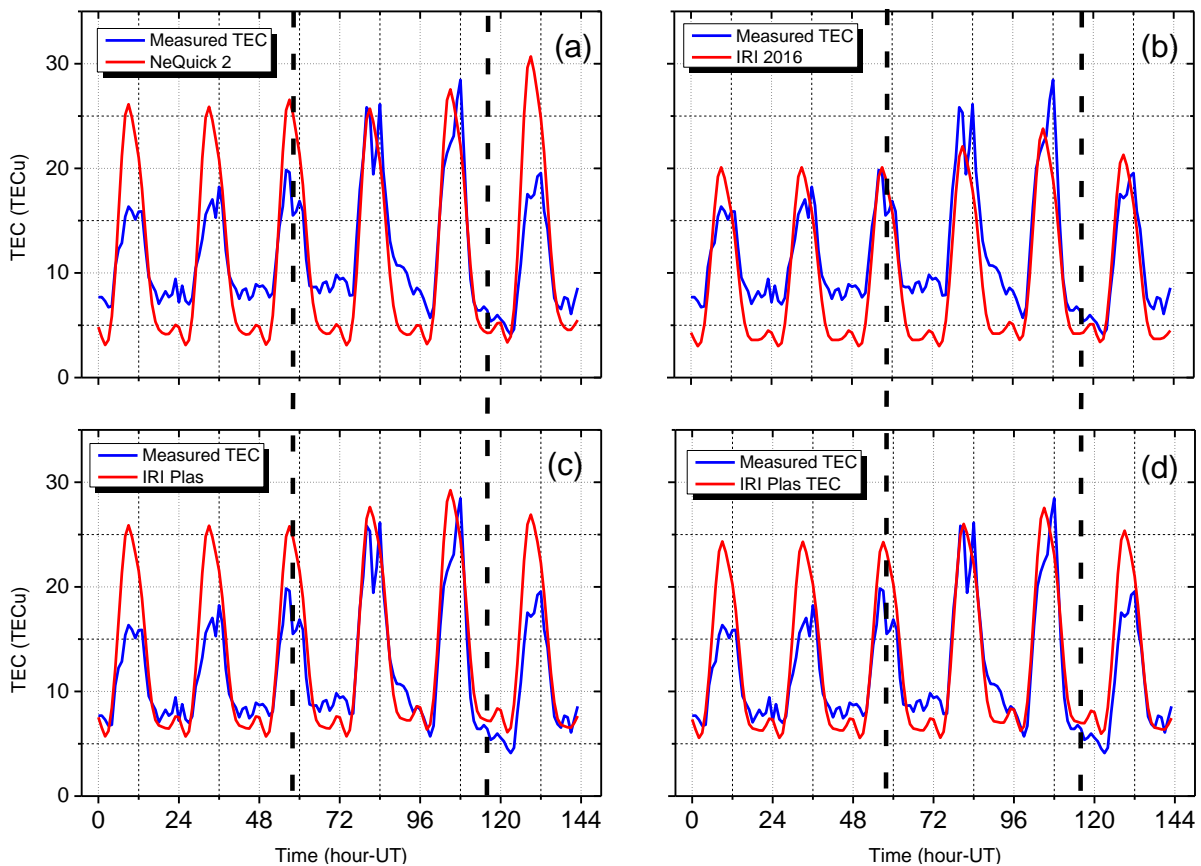


**Figure 9.** Variation of measured- NeQuick 2 TEC (a), Measured - IRI 2016 TEC (b), Measured - IRI Plas TEC (c), Measured - IRI Plas TEC (d) for the 3<sup>rd</sup> geomagnetic storm at Erzurum station. The duration between the dashed black lines indicates the storm time

**Table 6.** Comparison results for the 3<sup>rd</sup> geomagnetic storm process at Erzurum station

	Measured -NeQuick 2			Measured - IRI-2016			Measured - IRI-Plas			Measured - IRI-Plas (TEC)		
	pre-storm	during storm	post storm	pre-storm	during storm	post storm	pre-storm	during storm	post storm	pre-storm	during storm	post storm
MAE	4,22	3,32	4,03	3,22	3,65	2,28	3,24	2,30	3,24	2,77	2,10	2,67
RMSE	4,94	3,78	5,63	3,46	4,16	2,54	4,41	2,92	4,25	3,67	2,56	3,54
MAPE	38,45	30,21	34,36	34,62	32,68	25,61	25,36	18,57	33,22	22,62	17,29	28,41
KLD	0.176	0.110	0.106	0.136	0.083	0.075	0.061	0.039	0.035	0.055	0.036	0.035

**Analysis results for Istanbul station**

Figure 10 shows the time variation of the TEC values measured with the TEC values obtained from the empirical models for the 1<sup>st</sup> storm at the Istanbul station. The evaluation results of the model (by Equations (1), (2), (3) and (7)) are given in Table 7. When the measured TEC values with the NeQuick model were examined, it

was seen that the difference between the noon maximums before the storm continued during the storm period, while a good fit was obtained with the return phase of the storm. This is consistent in KLD value and metrics. While the IRI Plas and IRI Plas TEC models show good results pre-storm, the NeQuick 2 and IRI 2016 show good results post storm, and KLD and metrics show that they are compatible.

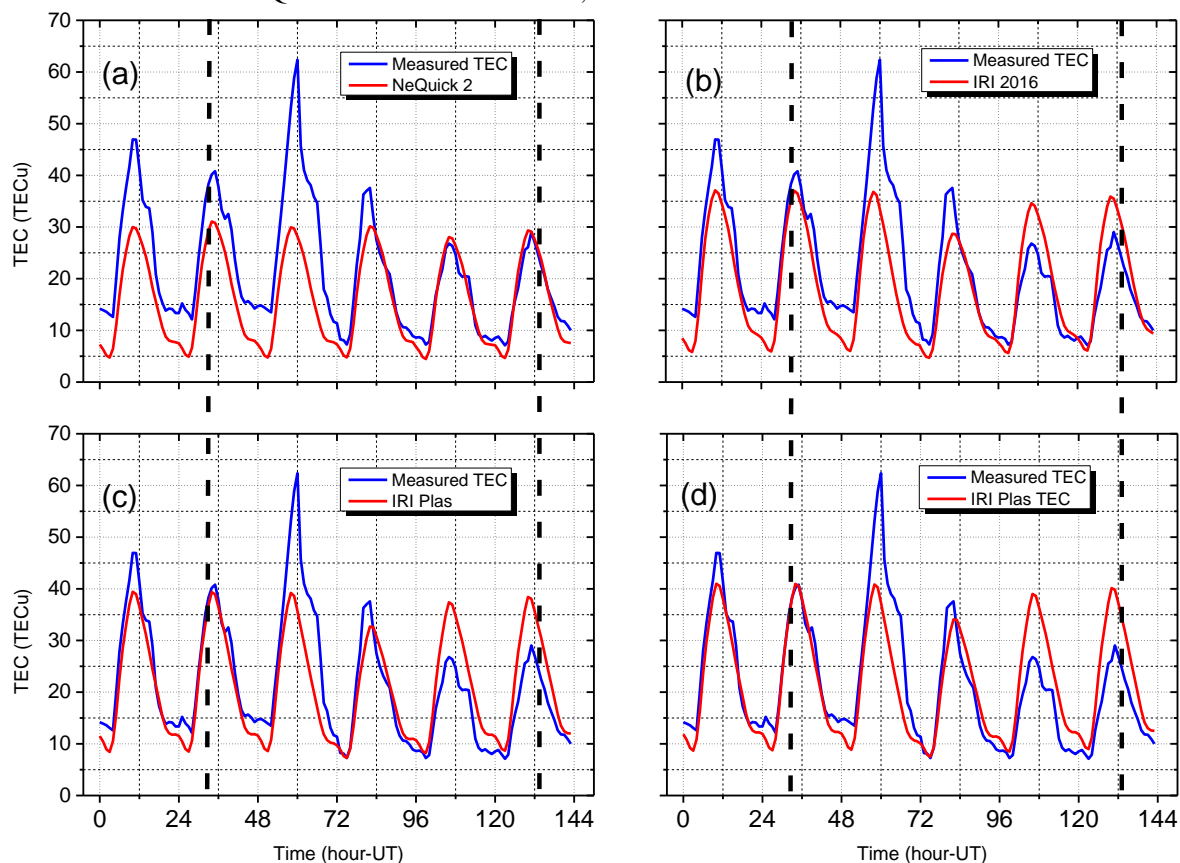


**Figure 10.** Variation of measured- NeQuick 2 TEC (a), Measured - IRI 2016 TEC (b), Measured - IRI Plas TEC (c), Measured - IRI Plas TEC (d) for the 1<sup>st</sup> geomagnetic storm at Istanbul station. The time duration between the dashed black lines indicates the storm time

**Table 8.** Comparison results for the 1<sup>st</sup> geomagnetic storm at Istanbul station

	Measured -NeQuick 2			Measured - IRI-2016			Measured - IRI-Plas			Measured - IRI-Plas (TEC)		
	pre-storm	during storm	post storm	pre-storm	during storm	post storm	pre-storm	during storm	post storm	pre-storm	during storm	post storm
MAE	9,01	6,18	0,88	5,73	5,71	0,29	3,50	5,26	0,34	2,89	5,31	0,49
RMSE	9,50	8,94	1,71	6,04	7,78	0,59	4,00	7,13	0,72	3,32	7,15	0,98
MAPE	42,43	26,48	15,17	29,33	25,23	17,59	16,62	24,30	27,92	14,29	25,63	34,09
KLD	0.030	0.088	0.015	0.032	0.095	0.015	0.011	0.083	0.023	0.012	0.079	0.027

The variation of the TEC values measured with the TEC values obtained from the empirical models for the 2<sup>nd</sup> storm at the Istanbul station is given in Figure 11. The evaluation results of the model (by means of Equations (1), (2), (3) and (7)) are given in Table 8. When the values measured with the NeQuick model were compared, it was understood from the KLD and metric results that it

gave good results especially after the storm and relatively good results before and during the storm. It is seen from the KLD value and metrics that the Measured TEC has a good relationship with IRI 2016 during post storm, IRI Plas (TEC) model values during pre-storm and storm times [19].

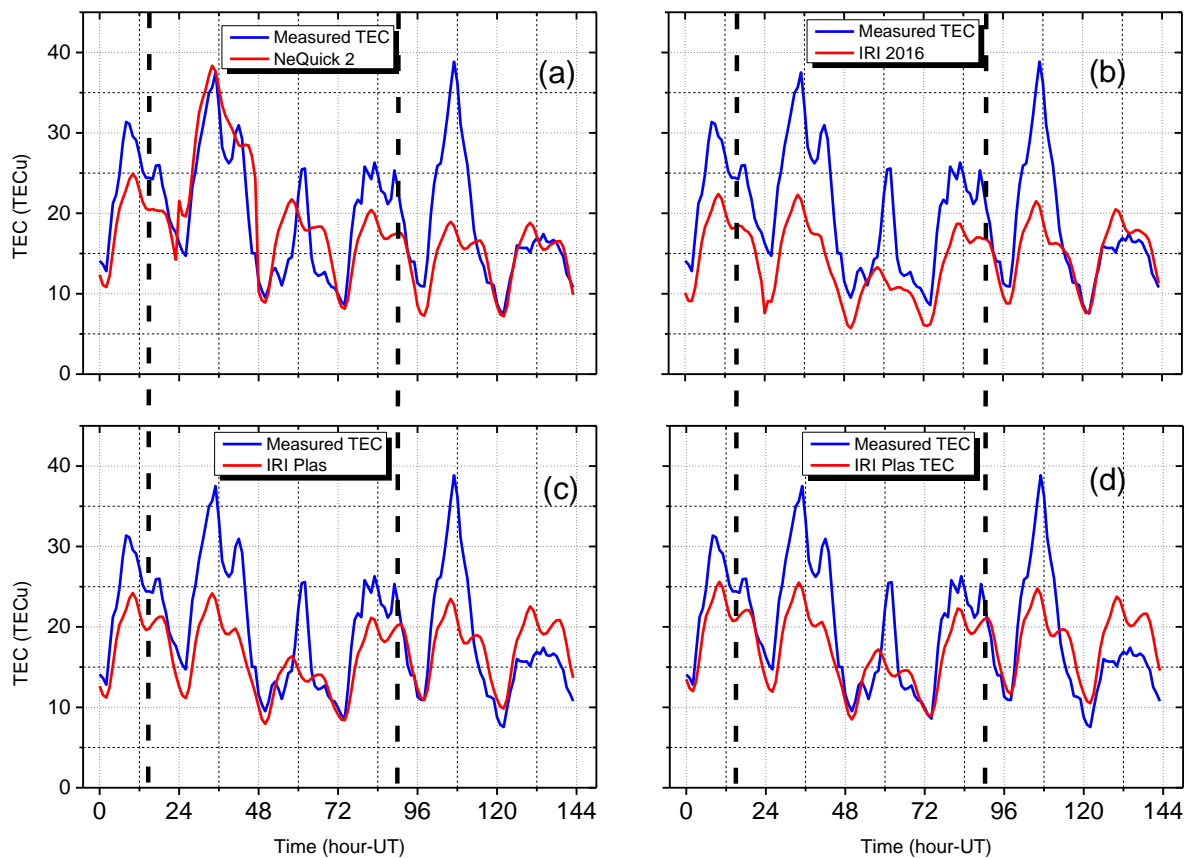


**Figure 11.** Variation of measured- NeQuick 2 TEC (a), Measured - IRI 2016 TEC (b), Measured - IRI Plas TEC (c), Measured - IRI Plas TEC (d) for the 2<sup>nd</sup> geomagnetic storm at Istanbul station. The time duration between the dashed black lines indicates the storm time

**Table 8.** Comparison results for the 2<sup>nd</sup> geomagnetic storm at Istanbul station

	Measured -NeQuick 2			Measured - IRI-2016			Measured - IRI-Plas			Measured - IRI-Plas (TEC)		
	pre-storm	during storm	post storm	pre-storm	during storm	post storm	pre-storm	during storm	post storm	pre-storm	during storm	post storm
MAE	4,91	4,20	4,32	7,34	6,95	3,96	5,35	4,85	4,51	4,18	4,21	4,87
RMSE	5,10	4,83	6,85	7,37	7,94	6,05	5,60	6,00	5,76	4,52	5,34	5,74
MAPE	20,66	23,05	19,28	31,51	32,59	17,77	21,90	21,40	23,84	16,76	18,64	27,53
KLD	0.003	0.057	0.087	0.003	0.028	0.036	0.003	0.033	0.082	0.004	0.033	0.081

In Figure 12, the variation of the TEC values measured and the TEC values obtained from the empirical models for the 3<sup>rd</sup> storm at the Istanbul station is shown. The evaluation results of the model (by Equations (1), (2), (3) and (7)) are given in Table 9. When the measured values with the NeQuick model values are examined (Figure 12a), it is seen that the NeQuick model predicts

exaggerated values. It is observed that these exaggerated values are compatible with the amount of increase in the TEC values measured by the storm. The best fit of the measured TEC can be seen from the KLD model and metric values that it provides with IRI 2016 during post storm.

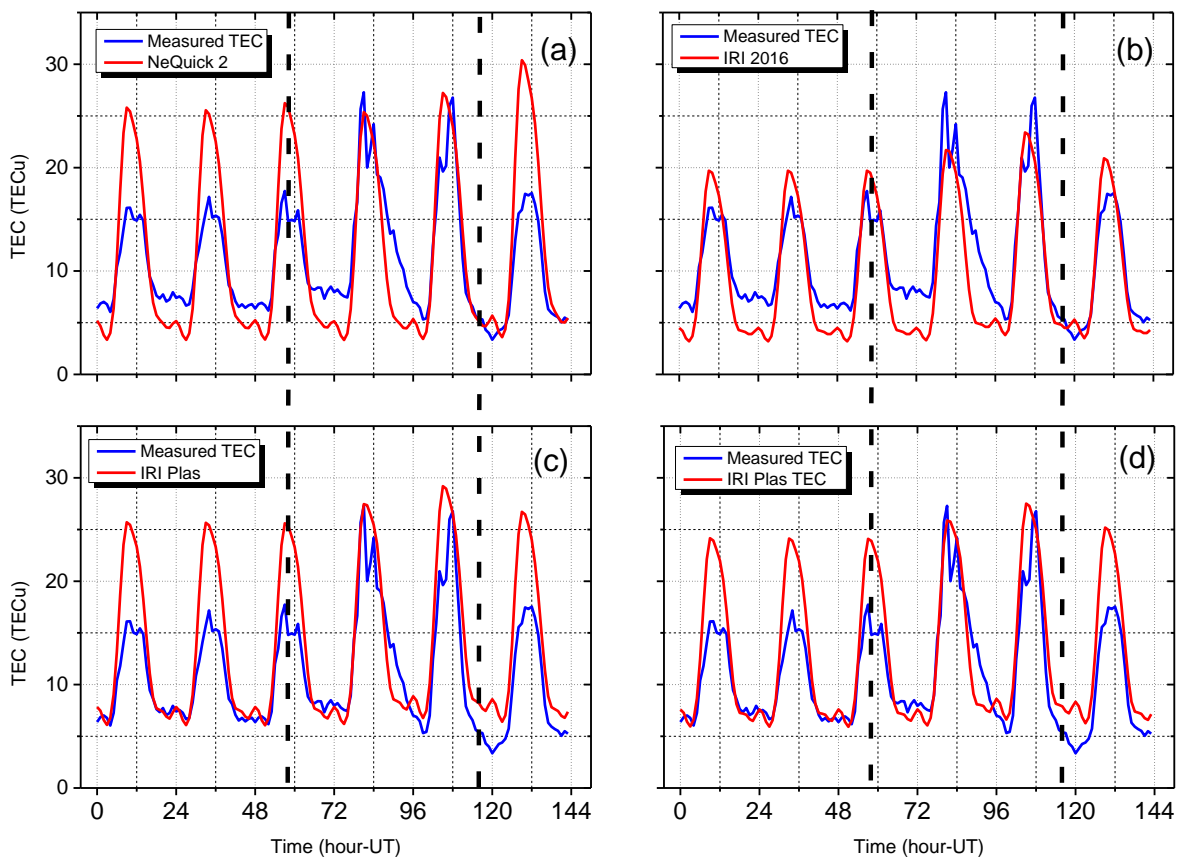


**Figure 12.** Variation of measured- NeQuick 2 TEC (a), Measured - IRI 2016 TEC (b), Measured - IRI Plas TEC (c), Measured - IRI Plas TEC (d) for the 3<sup>rd</sup> geomagnetic storm at Istanbul station. The duration between the dashed black lines indicates the storm time

**Table 9.** Comparison results for the 3<sup>rd</sup> geomagnetic storm at Istanbul station

	Measured -NeQuick 2			Measured - IRI-2016			Measured - IRI-Plas			Measured - IRI-Plas (TEC)		
	pre- storm	during storm	post storm	pre- storm	during storm	post storm	pre- storm	during storm	post storm	pre- storm	during storm	post storm
MAE	3,85	3,26	4,03	2,63	3,22	1,39	3,30	2,89	4,37	2,72	2,54	3,71
RMSE	4,85	3,95	5,99	2,80	3,84	1,74	4,81	3,76	5,00	3,99	3,20	4,24
MAPE	35,11	28,38	34,52	30,20	28,47	18,00	25,50	23,89	55,41	21,13	21,37	48,67
KLD	0.132	0.110	0.045	0.050	0.044	0.015	0.037	0.047	0.018	0.017	0.023	0.009

When the obtained results are compared with the literature, it is seen that consistent results are obtained. Tarıku Y., 2020 is calculated that the RMSE values obtained in the comparison of NeQuick, IRI 2016 and IRI Plas 2017 are compatible with the values obtained from the study[40]. However, Okah et al., 2018, compared to NeQuick and IRI Plas 2017, which is consistent with the low predicted result of the NeQuick model during the high solar activity period, but the opposite result was obtained with the lower predicted result of IRI Plas 2017[41]. In another study, it was stated that the IRI Plas model was better than the NeQuick model at low latitudes, and the NeQuick model was better at high latitudes[42].

## CONCLUSIONS

The change in TEC is one of the most important parameters in observing space weather, affecting satellite-based communication, positioning and navigation processes [43]. The TEC values are measured by satellite and GPS receivers, as well as estimated by models such as IRI and NeQuick. Model estimations are very important especially in regions where measurement is not made. In this context, in this study, the performance of empirical models was evaluated for three different severe geomagnetic storm processes that occurred in 2015, the beginning of the descending phase of the 24<sup>th</sup> solar cycle.

Although the NeQuick 2 model is climatically expressed [15], it seems to be the subject of many scientific studies (shown in the references section of this study). It is known that the IRI 2016 has a sub-option to choose from for the storm, while the NeQuick model does not. Among the empirical models, IRI Plas TEC was generally found to be better than other models for all storm processes. It can be stated that IRI 2016 is better in the storm recovery phase compared to other phases of the storm. From the study made, it can be stated that empirical model still needs to be developed for all stations and all storm processes.

## Acknowledgment

This submission is the extended version of the work presented in URSITR2021 and intended for the cluster related to this conference.

We would like to thank the IONOLAB group and TNPNG-Active, Turkish National Permanent GPS Network to founders for TEC data, the International GNSS Service for access to GNSS data used in this study; and the OMNIWeb Plus NASA/Goddard Space Flight Center service for the data on geomagnetic and solar flux indices.

This study has been studied as a Master's thesis at Institute of Science of Mus Alparslan University.

## REFERENCES

- [1] Jakowski N., Heise S., Stankov S. M. Tsybulya K. Remote sensing of the ionosphere by space-based GNSS observations. *Advances in Space Research*, 38(11), 2337–2343, 2006. doi:10.1016/j.asr.2005.07.015
- [2] Radicella S., Nava B. NeQuick model: Origin and evolution. *Annals of Geophysics*, 422–425, 2009. doi:10.1109/ISAPE.2010.5696491
- [3] Zhang Z., Moore J. C. Chapter 6 - Empirical Orthogonal Functions. *Mathematical and Physical Fundamentals of Climate Change*. Boston: Elsevier, 161–197, 2015. doi:10.1016/B978-0-12-800066-3.00006-1
- [4] Cooper C., Mitchell C. N., Wright C. J., Jackson D. R., Witvliet B. A. Measurement of Ionospheric Total Electron Content Using Single-Frequency Geostationary Satellite Observations, *Radio Science*, 54(1),10–19, 2019. doi: 10.1029/2018RS006575
- [5] Çetin K., Özcan O., Korlaelçi S. The interaction between stratospheric monthly mean regional winds and sporadic-E, *Chinese Physics B*, 26(3), 039401, 2017. doi:10.1088/1674-1056/26/3/039401
- [6] Bilitza D., Altadill D., Truhlik V., Shubin V., Galkin I., Reinisch B., Huang X. International Reference Ionosphere 2016: From ionospheric climate to real-time weather predictions, *Space Weather*,15(2), 418–429, 2017. doi: 10.1002/2016SW001593
- [7] Bilitza D. The International Reference Ionosphere 1990, National Space Science Data Center, NSSDC/WDC-AR &S Reports 90-22. 1990.
- [8] Bilitza D., Altadill D., Reinisch B., Galkin I., Shubin V., Truhlik V. The international reference ionosphere: model update 2016, *Geophysical Research Abstracts EGU General Assembly 2016*, EPSC2016-9671, 2016.
- [9] Bilitza D., Hernandez-Pajares M., Juan J., Sanz J. Comparison between IRI and GPS-IGS derived electron content during 1991–1997, *Physics and Chemistry of the Earth, Part C: Solar, Terrestrial & Planetary Science*, 24(4),311–319, 1999.

- [10] Gulyaeva T., Arikan F., Stanislawski I. Inter-hemispheric imaging of the ionosphere with the upgraded IRI-Plas model during the space weather storms, Earth, planets and space, 63(8), 929–939, 2011.
- [11] Tuna H., Arikan O., Arikan F., Gulyaeva T. L., Sezen U. Online user-friendly slant total electron content computation from IRI-Plas: IRI-Plas-STEAC, Space weather, 12(1), 64–75, 2014.
- [12] Sezen U., Gulyaeva T. L., Arikan F. Performance of Solar Proxy Options of IRI-Plas Model for Equinox Seasons, Journal of Geophysical Research: Space Physics, 123(2), 1441–1456, 2018. doi: 10.1002/2017JA024994
- [13] Han L., Wang J., Liu J. NeQuick Model Algorithm Research and Performance Assessment, Geomatics and Information Science of Wuhan University, 43, 464–470, 2018. doi:10.13203/j.whugis20150111
- [14] Wang N., Yuan Y., Li Z., Li Y., Huo X., Li M. An examination of the Galileo NeQuick model: comparison with GPS and JASON TEC, GPS Solutions, 21, 2017. doi:10.1007/s10291-016-0553-x
- [15] Nava B., Radicella S., Azpilicueta F. Data ingestion into NeQuick 2, Radio Science, 46, 2011. doi:10.1029/2010RS004635
- [16] Atiq M., Ameen M., Sadiq N., Khursheed H., Ali M., Yu X., Ameer A. Estimating foF<sub>2</sub> from GPS TEC over Islamabad and Darwin using NeQuick2 during 2011-2014. Advances in Space Research. 67, 1559–1569, 2021. doi:10.1016/j.asr.2020.12.003
- [17] Leitinger R., Zhang M.L., Radicella S. An improved bottomside for NeQuick, In EGS-AGU-EUG Joint Assembly, 1 Apr., 2003.
- [18] Nava B., Coisson P., Radicella S.M. A new version of the NeQuick ionosphere electron density model, Journal of Atmospheric and Solar-Terrestrial Physics, 70(15), 1856–1862, 2008. doi: 10.1016/j.jastp.2008.01.015
- [19] Atıcı R., Sağır S., Emelyanov L.Y., Lyashenko M. Investigation of Ionospheric Electron Density Change During Two Partial Solar Eclipses and Its Comparison with Predictions of NeQuick 2 and IRI-2016 Models. Wireless Personal Communications, 118(4), 2239–2251, 2021. doi:10.1007/s11277-021-08122-x
- [20] Jamjareegulgarn P., Ansari K., Ameer A. Empirical orthogonal function modelling of total electron content over Nepal and comparison with global ionospheric models. Acta Astronautica. 177, 497–507, 2020.
- [21] Karatay S., Arikan F., Arikan O. Investigation of total electron content variability due to seismic and geomagnetic disturbances in the ionosphere. Radio Science. 45(5), 2010. doi: 10.1029/2009RS004313
- [22] Deviren M.N., Arikan F., Arikan O. Spatio-temporal interpolation of total electron content using a GPS network, Radio Science, 48(3), 302–309, 2013. doi: 10.1002/rds.20036
- [23] Sezen U., Arikan F., Arikan O., Ugurlu O. Sadeghimorad A. Online, automatic, near-real time estimation of GPS-TEC: IONOLAB-TEC, Space Weather, 11(5), 297–305, 2013. doi:10.1002/swe.20054
- [24] Arikan F., Nayir H., Sezen U., Arikan O. Estimation of single station interfrequency receiver bias using GPS-TEC, Radio Science, 43(4), 2008. doi: 10.1029/2007RS003785
- [25] Bilitza D. IRI the International Standard for the Ionosphere, Advances in Radio Science, 16, 1–11, 2018. doi:10.5194/ars-16-1-2018
- [26] Sezen U., Gulyaeva T.L., Arikan F. Online computation of International Reference Ionosphere Extended to Plasmasphere (IRI-Plas) model for space weather. Geodesy and Geodynamics. 9(5), 347–357, 2018. doi: 10.1016/j.geog.2018.06.004
- [27] Gulyaeva T.L., Arikan F., Sezen U., Poustovalova L.V. Eight proxy indices of solar activity for the International Reference Ionosphere and Plasmasphere model, Journal of Atmospheric and Solar-Terrestrial Physics, 172, 122–128, 2018. doi: 10.1016/j.jastp.2018.03.025
- [28] Chai T., Draxler R. Root mean square error (RMSE) or mean absolute error (MAE)? Geoscientific Model Development, 7, 2014. doi:10.5194/gmd-7-1525-2014
- [29] Hall P. On Kullback-Leibler Loss and Density Estimation, The Annals of Statistics, 15(4), 1491–1519, 1987. doi:10.1214/aos/1176350606
- [30] Seghouane A.K., Amari S.I. The AIC Criterion and Symmetrizing the Kullback-Leibler Divergence, IEEE Transactions on Neural Networks, 18(1), 97–106, 2007. doi:10.1109/TNN.2006.882813
- [31] Astafyeva E., Zakharenkova I., Förster M. Ionospheric response to the 2015 St. Patrick's Day storm: A global multi-instrumental overview, Journal of Geophysical Research: Space Physics, 120(10), 9023–9037, 2015. doi: 10.1002/2015JA021629
- [32] Şentürk E. Investigation of global ionospheric response of the severe geomagnetic storm on June 22-23, 2015 by GNSS-based TEC observations, Astrophysics and Space Science, 365(7), 110, 2020. doi:10.1007/s10509-020-03828-z
- [33] Paul B., Gordiyenko G., Galav P. Study of the low and mid-latitude ionospheric response to the geomagnetic storm of 20th December 2015, Astrophysics and Space Science, 365(10), 174, 2020. doi:10.1007/s10509-020-03884-5
- [34] Özcan O., Sağır S., Atıcı R. The relationship between TEC and Earth's magnetic field during quiet and disturbed days over Istanbul, Turkey, Advances in Space Research. 65(9), 2167–2171, 2020.
- [35] Atıcı R., Aytaş A., Sağır S. The effect of solar and geomagnetic parameters on total electron content over Ankara, Turkey, Advances in Space Research. 65(9), 2158–2166, 2020.
- [36] Maurya A.K., Venkatesham K., Kumar S., Singh R., Tiwari P., Singh A.K. Effects of St. Patrick's Day geomagnetic storm of March 2015 and of June 2015 on low-equatorial D region ionosphere, Journal of Geophysical Research: Space Physics, 123(8), 6836–6850, 2018.
- [37] Macho E., Correia E., Paulo C., Angulo L., Vieira J. Ionospheric response to the June 2015 geomagnetic storm in the South American region, Advances in Space Research, 65, 2020. doi:10.1016/j.asr.2020.02.025
- [38] Cherniak I.V., Zakharenkova I. Large-Scale Traveling Ionospheric Disturbances Origin and Propagation: Case Study of the December 2015 Geomagnetic Storm, Space Weather. 16, 2018. doi:10.1029/2018SW001869
- [39] Mansilla G., Zossi M. Effects on the equatorial and low latitude thermosphere and ionosphere during the 19 – 22 December 2015 Geomagnetic storm period Advances in Space Research, 65, 2019. doi:10.1016/j.asr.2019.09.025
- [40] Tariku Y.A. Comparison of Performance of the IRI 2016, IRI-Plas 2017, and NeQuick 2 Models During Different Solar Activity (2013–2018) Years Over South American Sector, Radio Science, 55(8), e2019RS007047, 2020. doi: 10.1029/2019RS007047
- [41] Okoh D., Onwuneme S., Seemala G., Jin S., Rabiou B., Nava B., Uwamahoro J. Assessment of the NeQuick-2 and IRI-Plas 2017 models using global and long-term GNSS measurements, Journal of Atmospheric and Solar-Terrestrial Physics, 170:1–10, 2018. doi: 10.1016/j.jastp.2018.02.006
- [42] Ezquer R.G., Scidá L.A., Orué Y.M., Nava B., Cabrera M.A., Brunini C. NeQuick 2 and IRI Plas VTEC predictions for low latitude and South American sector. Advances in Space Research, 61(7), 1803–1818, 2018. doi: 10.1016/j.asr.2017.10.003
- [43] Deviren M., Arikan F. IONOLAB-MAP: An automatic spatial interpolation algorithm for total electron content, Turkish Journal of Electrical Engineering & Computer

Sciences, 26, 1933–1945, 2018. doi:10.3906/elk-1611-231